Electromagnetic fields and transmission properties in tapered hollow metallic waveguides

Xiahui Zeng[*] and Dianyuan Fan

Shanghai Institute of Optics and Fine mechanics, Chinese Academy of Science, Shanghai 201800, P R China
[*]Corresponding author: xiahuiz@126.com

Abstract: We analyze the electromagnetic spatial distributions and address an important issue of the transmission properties of spherical transverse-electric (TE) and transverse-magnetic (TM) eigenmodes within a tapered hollow metallic waveguide in detail. Explicit analytical expressions for the spatial distributions of electromagnetic field components, attenuation constant, phase constant and wave impedance are derived. Accurate eigenvalues obtained numerically are used to study the dependences of the transmission properties on the taper angle, the mode as well as the length of the waveguide. It is shown that all modes run continuously from a propagating through a transition to an evanescent region and the value of the attenuation increases as the distance from the cone vertex and the cone angle decrease. A strict distinction between pure propagating and pure evanescent modes cannot be achieved. One mode after the other reaches cutoff in the tapered hollow metallic waveguide as the distance from the cone vertex desreases.

©2008 Optical Society of America

OCIS code: (230.7380) Waveguides,channeled; (130.2790) Guide waves; (350.5500) Propagation; (030.4070) Modes; (000.4430) Numerical approximation and analysis.

References and Links

1. Z. Wang, M. Dai, and J. Yin, "Atomic (or molecular) guiding using a blue-detuned doughnut mode in a hollow metallic waveguide," Opt. Express **13**, 8406-8423 (2005).
2. S. S. Lo and C. C. Chen, "1×2 multimode interference couplers based on semiconductor hollow waveguides formed from omnidirectional reflectors," Opt. Lett. **32**, 1803-1805 (2007).
3. N. Ponnampalam and R. G. DeCorby, "Out-of-plane coupling at mode cutoff in tapered hollow waveguides with omnidirectional reflector claddings," Opt. Express **16**, 2894-2908 (2008).
4. P. D. Potter, "A new horn antenna with suppressed sides lobes and equal beamwidth," Microwave J. **6**, 71-78 (1963).
5. M. S. Narasimhan and K. S. Balasubramanya, "Transmission characteristics of spherical TE and TM modes in conical waveguides," IEEE Trans. Microwave Theory and Techniques **17**, 965-970 (1974).
6. J. Kim and K. B. Song, "Recent progress of nano-technilogy with NSOM," Micron **38**, 409-426 (2007).
7. T. J. Antosiewicz and T. Szoplik, "Corrugated metal-coatedtapered tip for scanning near-field optical microscope," Opt. Express **15**, 10920-10928 (2007).
8. M. H. Key, J. C. Adam, K. U. Akli, M. Borghesi, M. H. Chen, R. G Evans, R. R. Freeman, H. Habara, S. P. Hatchett, J. M. Hill, A. Heron, J. A. King, R. Kodama, K. L. Lancaster, A. J. MacKinnon, P. Patel, T. Phillips, L. Romagnani, R. A. Snavely, R. Stephens, C. Stoeckl, R. Town, Y. Toyama, B. Zhang, M. Zepf, and P. A. Nrreys, "Fast ignition relevant study of the flux of high intensity laser-generated electrons via a hollow cone into a laser-imploded plasma," Phys. Plasma **15**, 022701 (2008).
9. Y. Sentoku, K. Mima, H. Ruhl, Y. Toyama, R. Kodama, and T. E. Cowan, "Laser light and hot electron micro focusing using a conical target," Phys. Plasma **11**, 3083-3087 (2004).
10. L. Novotny and C. Hafner, "Light propagation in a cylindrical waveguide with a complex, metallic, dielectric function," Phys. Rev. E **50**, 4094-4106 (1994).
11. R. F. Harrington, *Time-harmonic electomagnetic fields* (Wiley-IEEE, 2001), Chap. 6.
12. S. Narita, Y. Matsuura, and M. Miyagi, "Tapered hollow waveguide for focusing infrared laser beams," Opt. Lett. **32**, 930-932 (2007).
13. E. X. Jin and X. Xu, "Obtaining super resolution light spot using surface plasmon assisted sharp ridge nanoaperture," Appl. Phys. Lett. **86**, 111106 (2005).

1. Introduction

The advent of high–purity ultra-low-loss silica fiber as a transmission medium in the late 1970s provided a basis for the modern optical communication infrastructure. Although highly successful, silica waveguides have fundamental limitations in the their attenuation and nonlinearities that result from the interaction of light with a dense, material-filled core. A different approach to waveguiding circumvents these problems by confining light in a hollow core using highly reflective walls. This approach is exemplified by hollow waveguides with perfectly conducting metallic wall [1] and omnidirectional reflector claddings [2, 3]. Prior to the emergence of sillica fiber, the hollow conical waveguides (horns) have got successful applications in many fields such as millimeter-wave communication, microwave radio-relay links, and satellite communication [4, 5]. They have been mainly used as a simple and compact antenna structure. In recent years, hollow metallic waveguides with a conical taper have been investigated in view of their applicability as couplers. These waveguides find some important applications in optical communication, scanning near-field optical microscopy, and laser-wakefield accelerators [6-9]. A threoretical treatment of a tapered optical waveguide presents formidable mathematical difficulties. One can not but , therefore, have recourse to approximate methods. A typical approach is to assume the tapered hollow metallic waveguides as a stack of a large number of optical waveguides of increasing cross-sectional size arranged end to end [10]. However, the actual electromagnetic fields configurations, their transmission characteristics, as welll as impedance and fields intensities distributions have not been thoroughly investigated.

In the present paper, we report the results of a theoretical investigation of a tapered hollow metallic waveguide from a exact analytical approach. Some numerical solutions based on a discretization are used to overcome the difficulties involed in finding the accurate eigenvalues of this boundary value problem and the evaluation of the associated eigenfunctions. A detailed study of the electromagnetic fields configurations, their transmission characteristics, as well as impedance and fields intensities distributions inside a conical hollow metallic waveguides is facilitated by accurate computation of eigenvalues. Explicit expressions for the field components, attenuation constant, phase constant, wave impedance and field intensity are obtained for the spherical TE and TM modes in a perfectly conducting conical hollow waveguide.

2. Spatial distributions of electromagnetic fields for the spherical TE and TM modes

Here we discuss the behaviour of electromagnetic fields inside a truncated cone of circular cross-sectional shape with perfectly conducting metallic walls and with a loss-free air core. A meridional and a transverse section of such a waveguide can be seen in Figs. 1(a) and 1(b). Throughout this paper we consider time-harmonic dependence of the fields. Further, we omit the factor $\exp(-i\omega t)$ from all expressions. In spherical coordinates (r, θ, φ) the basic equation for the Hertz function $U(r, \theta, \varphi)$ of electromagnetic fields in conical waveguide can be written as [11]

$$\frac{\partial^2 U}{\partial r^2} + \frac{1}{r^2}\left[\frac{1}{\sin\theta}\frac{\partial}{\partial\theta}\left(\sin\theta\frac{\partial U}{\partial\theta}\right) + \frac{1}{\sin^2\theta}\frac{\partial^2 U}{\partial\varphi^2}\right] + k^2 U = 0\,. \tag{1}$$

Here r is the distance from the cone vertex, θ and φ are polar and azimuthal angles, respectively. $k = 2\pi/\lambda = \omega/v$ is wave number (ω and v are the frequency and the velocity of light respectively, and λ denotes its wavelength in air).
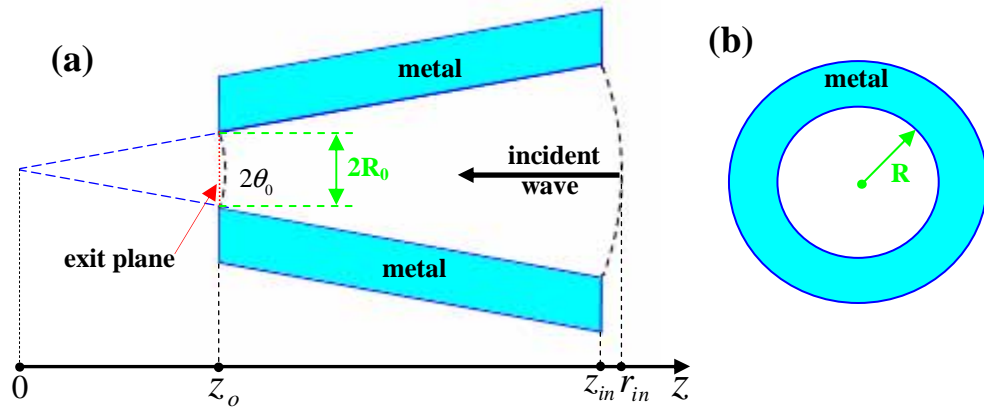
Fig. 1. Schematic illustrating a conical hollow metallic waveguide. (a) Meridional section of hollow metallic waveguide with a taper. The apex of the cone coincides with the origin of the spherical coordinate system. $2\theta_0$ is the cone angle, z_0 is the longitudinal coordinate at the waveguide exit, $2R_0$ is the aperture diameter in the exit plane, r_{in} and $z_{in} = r_{in}\cos\theta_0$ are the radial and longitudinal coordinates at the waveguide entrance, respectively. (b) Transverse section of hollow metallic waveguide with a taper. R presents transverse section radius and $R = r\sin\theta_0$.

If the apex of the cone coincides with the origin of the spherical coordinate system and polar axis is the longitudial axis of symmetry of the cone, then conical surface will coincide with surface of constant colatitude as shown in Fig. 1(a). The field components of the permissible TE modes to r can be expressed in terms of the Hertz function U by means of the following relations [11]:

$$E_r = 0$$

$$E_\theta = -\frac{1}{r\sin\theta}\frac{\partial U(r,\theta,\varphi)}{\partial \varphi} = \frac{1}{r}R(r)\frac{m}{\sin\theta}P_l^m(\cos\theta)\sin m\varphi ,\qquad (2)$$

$$E_\varphi = \frac{1}{r}\frac{\partial U(r,\theta,\varphi)}{\partial \theta} = \frac{1}{r}R(r)\frac{\partial}{\partial \theta}[P_l^m(\cos\theta)]\cos m\varphi$$

$$H_r = \frac{1}{j\omega\mu}(k^2 + \frac{\partial^2}{\partial r^2})U(r,\theta,\varphi) = \frac{1}{j\omega\mu}(k^2 + \frac{\partial^2}{\partial r^2})R(r)P_l^m(\cos\theta)\cos m\varphi$$

$$H_\theta = \frac{1}{j\omega\mu}\frac{\partial^2 U(r,\theta,\varphi)}{r\partial r\partial\theta} = \frac{1}{j\omega\mu}\left[\frac{1}{r}\frac{\partial}{\partial r}R(r)\right]\frac{\partial}{\partial\theta}[P_l^m(\cos\theta)]\cos m\varphi \qquad . \quad (3)$$

$$H_\varphi = \frac{1}{j\omega\mu}\frac{1}{r\sin\theta}\frac{\partial^2 U(r,\theta,\varphi)}{\partial r\partial\varphi} = \frac{1}{j\omega\mu}\left[\frac{1}{r}\frac{\partial}{\partial r}R(r)\right]\frac{-m}{\sin\theta}P_l^m(\cos\theta)\sin m\varphi$$

Note that E_r, E_θ, E_φ and H_r, H_θ, H_φ denote the components of the electric **E** and magnetic **H** fields associated with the corresponding spherical coordinates r,θ,φ . Where $R(r) = kr\cdot h_l^{(1)}(kr)$, $h_l^{(1)}(kr)$ is the spherical Bessel function of the third kind with a noninteger index l , corresponding to the inward-traveling wave, and $P_l^m(\cos\theta)$ is the associated Legendre function of order l and degree m . The azimuthal symmetry sets m as

an integer. l is determined by the bounary condition $\mathbf{n} \times \mathbf{E} = 0$ which yields $E_\varphi(\theta_0) = 0$ for the tangential component of the electric field $\mathbf{E}$ on the boundary between a hollow core and a perfectly conducting metallic surface of a cone. With the help of Eq. (2), the boundary condition for TE waves can be rewritten in terms of the associated Legendre function

$$\frac{d}{d\theta}\left[P_l^m(\cos\theta) \right]\bigg|_{\theta=\theta_0} = 0 . \tag{4}$$

For TM modes to r, one can use the above notation for the Hertz function U, where U obeys the Eq. (1). In this case the field components inside conical waveguides can be written as [11]

$$E_r = \frac{1}{j\omega\varepsilon}(k^2 + \frac{\partial^2}{\partial r^2})U(r,\theta,\varphi) = \frac{1}{j\omega\varepsilon}(k^2 + \frac{\partial^2}{\partial r^2})R(r)P_l^m(\cos\theta)\cos m\varphi$$

$$E_\theta = \frac{1}{j\omega\varepsilon}\frac{\partial^2 U(r,\theta,\varphi)}{r\partial r\partial\theta} = \frac{1}{j\omega\varepsilon}\left[\frac{1}{r}\frac{\partial}{\partial r}R(r)\right]\frac{\partial}{\partial\theta}[P_l^m(\cos\theta)]\cos m\varphi \qquad , \tag{5}$$

$$E_\varphi = \frac{1}{j\omega\varepsilon}\frac{1}{r\sin\theta}\frac{\partial^2 U(r,\theta,\varphi)}{\partial r\partial\varphi} = \frac{1}{j\omega\varepsilon}\left[\frac{1}{r}\frac{\partial}{\partial r}R(r)\right]\frac{-m}{\sin\theta}P_l^m(\cos\theta)\sin m\varphi$$

$$H_r = 0$$

$$H_\theta = \frac{1}{r\sin\theta}\frac{\partial U(r,\theta,\varphi)}{\partial\varphi} = \frac{1}{r}R(r)\frac{-m}{\sin\theta}P_l^m(\cos\theta)\sin m\varphi . \tag{6}$$

$$H_\varphi = -\frac{1}{r}\frac{\partial U(r,\theta,\varphi)}{\partial\theta} = \frac{1}{r}R(r)[-\frac{\partial}{\partial\theta}P_l^m(\cos\theta)]\cos m\varphi$$

Where the bounary condition $\mathbf{n} \times \mathbf{E} = 0$ yields $E_\varphi(\theta_0) = 0$ and $E_r(\theta_0) = 0$ for the tangential component of the electric field $\mathbf{E}$ at an interface. With the help of Eq. (5), the boundary condition for TM waves can be rewritten in terms of the associated Legendre function

$$P_l^m(\cos\theta)\big|_{\theta=\theta_0} = 0 . \tag{7}$$

The Eq. (4) yields a set of eigenvalues l_{mn} associated with the TE_{mn} field modes. For a given azimuthal number m ($m = 0, 1, 2, \ldots$), the index n ($n = 1, 2, 3, \ldots$) denotes the corresponding root of Eq. (4). Similarly, each choice of a pair (m, n) in Eq. (7) determined a possible TM_{mn} field mode. The eigenvalues l_{mn} of Eqs. (4) and (7) depend upon the cone half-angle θ_0, such that l_{mn} increases as the magnitude of θ_0 decreases. In the table 1 we give the values of l_{mn} for the first 5 lowest-order modes ($TE_{11}, TM_{01}, TE_{21}, TM_{11}, TE_{01}$) determined by Eqs. (4) and (7).

Table 1. The eigenvalues l_{mn} for the $TE_{11}, TM_{01}, TE_{21}, TM_{11}, TE_{01}$ modes as functions of the cone half-angle θ_0.

θ_0	$\pi/24$	$\pi/12$	$\pi/6$	$\pi/4$	$\pi/3$	$\pi/2$
$l_{mn}(\theta_0)$ TE_{11}	13.5914	6.5817	3.1204	2.0000	1.4684	1.0000
$l_{mn}(\theta_0)$ TM_{01}	18.0217	8.6743	4.0932	2.5481	1.8361	1.0000
$l_{mn}(\theta_0)$ TE_{21}	22.8573	11.2857	5.6046	3.6567	2.7917	2.0000
$l_{mn}(\theta_0)$ TM_{11}	28.7754	14.1437	6.8335	4.4011	3.2012	2.0000
$l_{mn}(\theta_0)$ TE_{01}	28.7754	14.1437	6.8335	4.4011	3.2012	2.0000

3. Transmission characteristics of the spherical TE and TM modes inside conical hollow metallic waveguide

The transmission properties of the guide modes are governed by a number of physical quantities. The important parameters are the attenuation and phase constants which are defined as the logarithmic rate of decrease of amplitude and phase, respectively, of a field component in the direction of propagation. More interesting, however, is the electric field component. For all electric field components of the spherical TE and TM modes mentioned previously, one can expressed them as

$$E(r,\theta,\varphi) = A(\theta,\varphi)e^{jk_r r}, \tag{8}$$

where E represents E_r, E_θ or E_φ for TE or TM modes, $A(\theta,\varphi)$ is real, and k_r is the propagation constant in the direction r and complex. With the help of Eq. (8), we can obtain

$$jk_r = -\frac{1}{E}\frac{\partial E}{\partial r}. \tag{9}$$

Further, we introduce the following quantity:

$$\gamma(\alpha,\beta) = \alpha + j\beta = -\frac{1}{E}\frac{\partial E}{\partial r}. \tag{10}$$

Substituting this into Eqs. (8) and (9), we can obtain

$$E(r,\theta,\varphi) = A(\theta,\varphi)e^{j(-\beta+j\alpha)r} = A(\theta,\varphi)e^{-\alpha r - j\beta r}, \tag{11}$$

where α is defined as the attenuation and β as the phase constant and α, β are real. If $\beta < 0$, we have inward-traveling waves which are attentuated or augmented according as α is positive or negative.

For TE or TM modes inside the conical hollow metallic waveguide, and with the help of Eqs. (2), (5) and (10), one obtains

$$\gamma_{\theta,\varphi}^{TE}(r,l) = k[\tfrac{1}{2}\tfrac{1}{kr} - H_{l+\frac{1}{2}}^{\prime(1)}/H_{l+\frac{1}{2}}^{(1)}], \tag{12}$$

$$\gamma_{\theta,\varphi}^{TM}(r,l) = k\frac{\tfrac{3}{4}\tfrac{1}{kr}H_{l+\frac{1}{2}}^{(1)} - kr H_{l+\frac{1}{2}}^{\prime\prime(1)}}{\tfrac{1}{2}H_{l+\frac{1}{2}}^{(1)} + kr H_{l+\frac{1}{2}}^{\prime(1)}}, \tag{13}$$

and

$$\gamma_r^{TM}(r,l) = -\frac{k[4krH_{l+\frac{1}{2}}^{(1)} + 8k^2r^2H_{l+\frac{1}{2}}'^{(1)} + \frac{3}{kr}H_{l+\frac{1}{2}}^{(1)} - 6H_{l+\frac{1}{2}}'^{(1)} + 12krH_{l+\frac{1}{2}}''^{(1)} + 8k^2r^2H_{l+\frac{1}{2}}'''^{(1)}]}{8k^2r^2H_{l+\frac{1}{2}}^{(1)} - 2H_{l+\frac{1}{2}}^{(1)} + 8krH_{l+\frac{1}{2}}'^{(1)} + 8k^2r^2H_{l+\frac{1}{2}}''^{(1)}} . \qquad (14)$$

Where $H_{l+\frac{1}{2}}^{(1)}$ is the first kind Hankel function of order $l+0.5$ with the argument kr. $H_{l+\frac{1}{2}}'^{(1)}, H_{l+\frac{1}{2}}''^{(1)}$ and $H_{l+\frac{1}{2}}'''^{(1)}$ are the first, the second and the third derivatives of the Hankel function with the argument kr, respectively. The Hankel function function $H_{l+\frac{1}{2}}^{(1)}(kr)$ and its derivative can be expressed as complex quantities and the real and imaginary parts of $\gamma_{\theta,\varphi}^{TE}(r,l)$, $\gamma_{\theta,\varphi}^{TM}(r,l)$ and $\gamma_r^{TM}(r,l)$ give the attenuation and phase constants, respectively, for the TE to r and TM to r modes.

Another parameter of particular interest associated with the mode transmission is the wave impedance, defined by [11]

$$Z_r^{TE} = -\frac{E_\theta}{E_\varphi} = \frac{E_\varphi}{E_\theta} , \qquad (15)$$

$$Z_r^{TM} = -\frac{E_\theta}{E_\varphi} = \frac{E_\varphi}{E_\theta} . \qquad (16)$$

With the help of Eqs. (2), (5), (15) and (16), one can obtain

$$Z_r^{TE} = j\eta \frac{H_{l+\frac{1}{2}}^{(1)}(kr)}{\frac{1}{2}\frac{1}{kr}H_{l+\frac{1}{2}}^{(1)}(kr) + H_{l+\frac{1}{2}}'^{(1)}(kr)} , \qquad (17)$$

$$Z_r^{TM} = -j\eta \frac{\frac{1}{2}\frac{1}{kr}H_{l+\frac{1}{2}}^{(1)}(kr) + H_{l+\frac{1}{2}}'^{(1)}(kr)}{H_{l+\frac{1}{2}}^{(1)}(kr)} , \qquad (18)$$

where $\eta = \sqrt{\frac{\mu}{\varepsilon}}$ is called the intrinstic impedance of the medium.

4. The space variation of the attenuation and phase constants of the spherical TE and TM modes

Based on the Eqs. (12), (13) and (14), a variation of the attenuation α and phase constants β for the spherical TE and TM modes as a function of kr with cone half-angle θ_0 as a parameter has been studied and the results are presented in Figs. 2-5.
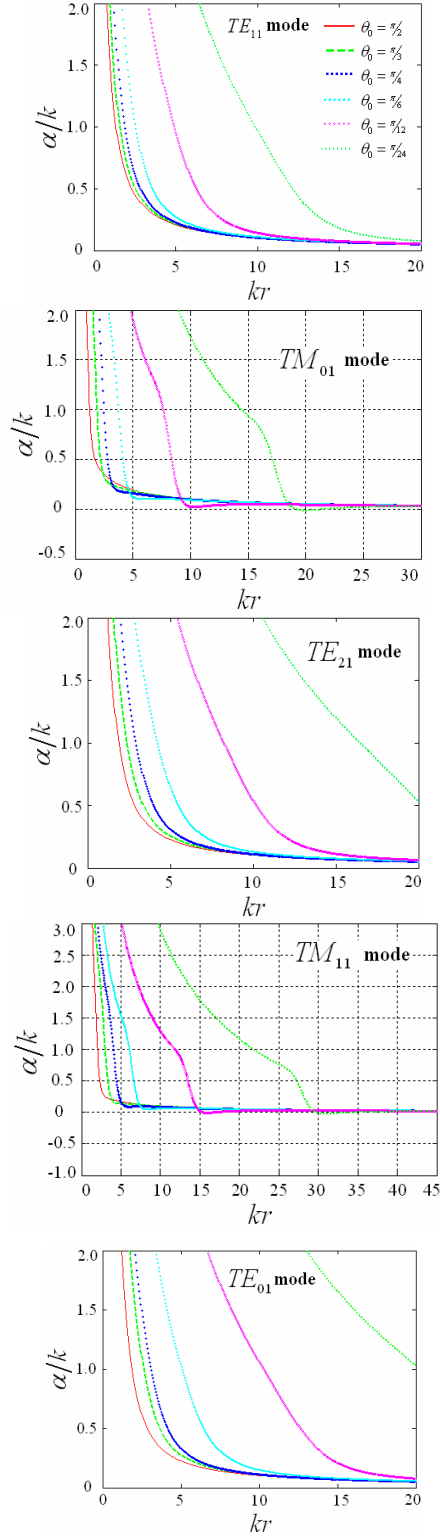
Fig. 2. The attenuation constant (α) of E_θ and E_φ for the TE and TM modes as a function of kr .
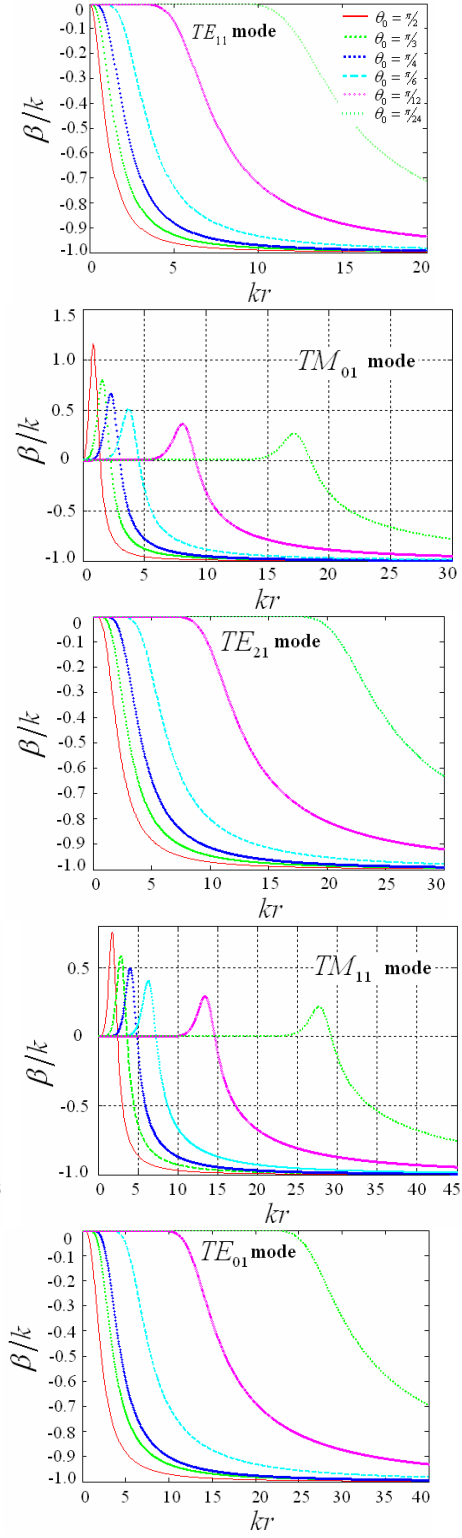
Fig. 3. The phase constant (β) of E_θ and E_φ for the TE and TM modes as a function of kr .
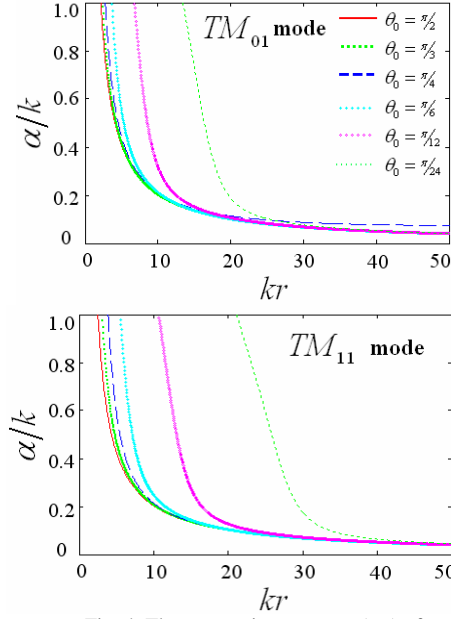
Fig. 4. The attenuation constant (α) of E_r for TM modes as a function of kr .
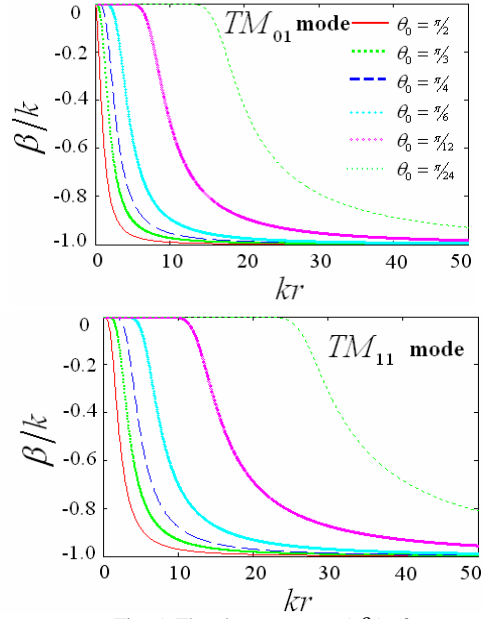
Fig. 5. The phase constant (β) of E_r for the TM modes as a function of kr .

Figures 2 and 3 show a variation of the attenuation α and phase constants β of E_θ and E_φ for the first 5 lowest-order modes as a function of kr with cone half-angle θ_0 as a parameter in the propagation direction, respectively. Figures 4 and 5 present α and β of E_r for the TM_{01} and TM_{11} modes as a function of kr with cone half-angle θ_0 as a parameter, respectively. As kr desreases all modes run continuously from a propagating through a transition to an evanescent region. We note that a strict distinction between pure propagating and pure evanescent modes can not be achieved. The value of the attenuation α increases and the phase constants β changes from $\approx -k$ to 0 as kr desreases. $\beta < 0$ represents inward-traveling wave and $\beta > 0$ represents outward-traveling wave which describes the reflection effect inside the conical hollow metallic waveguide. There is no well-defined cutoff wavelength but rather a cutoff radius (R_c). All modes have a cutoff when $\beta = 0$. However, it is interesting to note that the magnitude of the cutoff radius is related to the wavelength and the cone half-angle. At about $kr = 10$, for example, the TE_{11} reaches cutoff inside the tapered hollow waveguide with cone half-angle $\theta_0 = \pi/24$. By computation, we can obtain the cutoff radius $R_c = (5\lambda/\pi) \cdot \sin \pi/24 \approx 0.2077\lambda$. That is, the mode reaches cutoff at subwavelength-sized aperture. In the Figs 2-5, we observe the values of attenuation α and phase constants β depend on the cone half-angle θ_0 very seriously. As θ_0 decreases, the value of the attenuation increases. The smaller the cone half-angle is, the faster the modes attenuate. It is necessary to stress that our analysis is restrict to perfect metallic conductor only. While this approximation of real metallic walls with perfect electric conductors is applicable only for near infrared and lower frequencies, because metallic wavuguides become lossy at high frequencies due to the finite condutivity of metals.

Figure 6 shows α and β for the first 5 lowest-order modes as a function of kr with fixed cone half-angle $\theta_0 = \pi/6$ in the propagation direction. Note that a logarithmic scale is used in Fig. 6(a). In the propagating region the attentuation of some modes decays faster than

those of others. At $kr = 10$, for example, the TM_{11} mode shows the lowest attenuation. The sequence of modes of the cylindrical hollow metal waveguide starts with $TE_{11}, TM_{01}, TE_{21}, TM_{11}, TE_{01}$, and the latter two modes TM_{11} and TE_{01} are degenerate. Whereas for the conical hollow metallic waveguide we can obtain sequence $TM_{11}, TM_{01}, TE_{11}, TE_{21}, TE_{01}$ beyond $kr \approx 7.5$. The TM_{11} and TE_{01} modes are not degenerate. From the Fig. 6(b), we observe that one mode after the other reaches cutoff in the tapered hollow metallic waveguide as kr decreases.
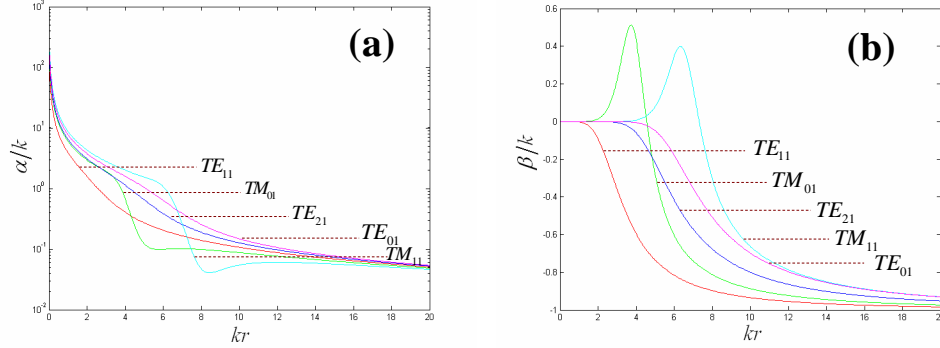

Fig. 6. Variation of the attenuation α and phase constants β for the first 5 lowest-order modes as a function of kr with cone half-angle $\theta_0 = \pi/6$ as a parameter.

5. Radial dependences of the wave impedance for the spherical TE and TM modes

We shall consider below the main features in the behaviour of the wave impedance as a function of kr for the spherical TE and TM modes inside the conical hollow metallic waveguide. Based on the Eqs. (17) and (18), a variation of the the wave impedance for TE_{11} and TM_{01} modes as a function of kr with cone half-angle θ_0 as a parameter has been studied and the results are presented in Fig. 7. By numerical simulations we find the magnitude of the absolute values for the wave impedances $\left| Z_r^{TE} \right|$ and $\left| Z_r^{TM} \right|$ depend on the cone half-angle θ_0 and kr.
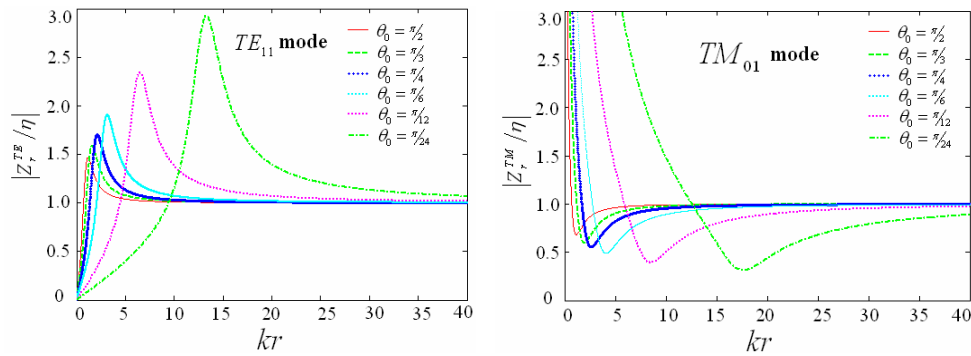
Fig. 7. The absolute value of the wave impedance $\left| Z_r^{TE} \right|$ and $\left| Z_r^{TM} \right|$ as a function of kr for the spherical TE and TM modes inside the conical hollow metallic waveguide.

6. Electromagnetic fields configurations and fields intensities distributions within tapered hollow metal waveguide

In this section we consider the electromagnetic fields configurations and fields intensities distributions inside tapered hollow metal waveguide. To provide a better understanding of the

fields configurations for the spherical TE and TM modes, in Fig. 8 the electric-field time-average engergy density $\frac{1}{2}\varepsilon|\mathbf{E}|^2$ is plotted for the $TE_{11}, TM_{01}, TE_{21}, TM_{11}, TE_{01}$ modes at a wavelength $\lambda = 1.06\mu m$, the distance from the cone vertex $r = 20mm$ and a cone half-angle $\theta_0 = \pi/6$. We find that the modes configurations are similar to those of the cylindrical hollow metal waveguide for which completely transverse modes are obtained.
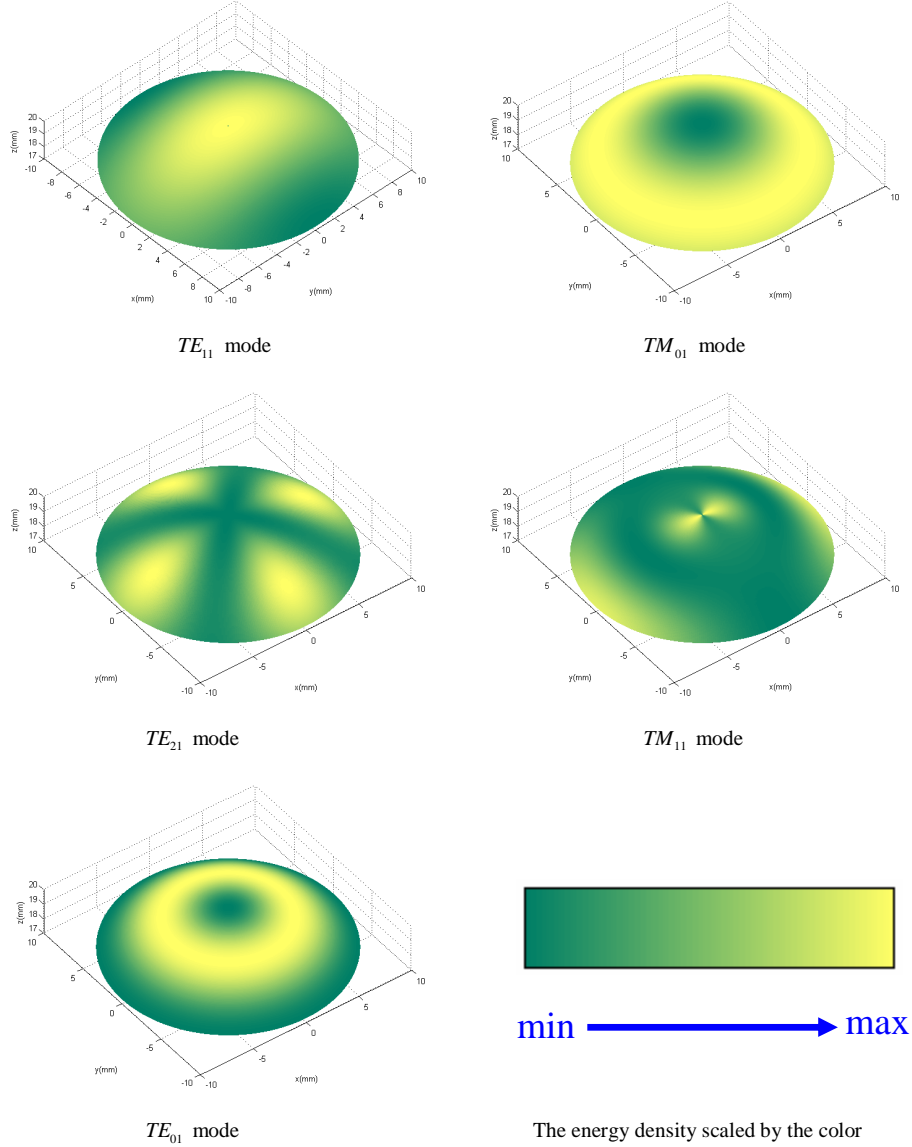
TE_{11} mode

TM_{01} mode

TE_{21} mode

TM_{11} mode

TE_{01} mode

The energy density scaled by the color

Fig. 8. The electric-field time-average engergy density for the first 5 modes is shown in the spherical cross section with the radius $r = 20mm$. The color scheme is such that the engergy density goes from minimum (green) to maximum (yellow).
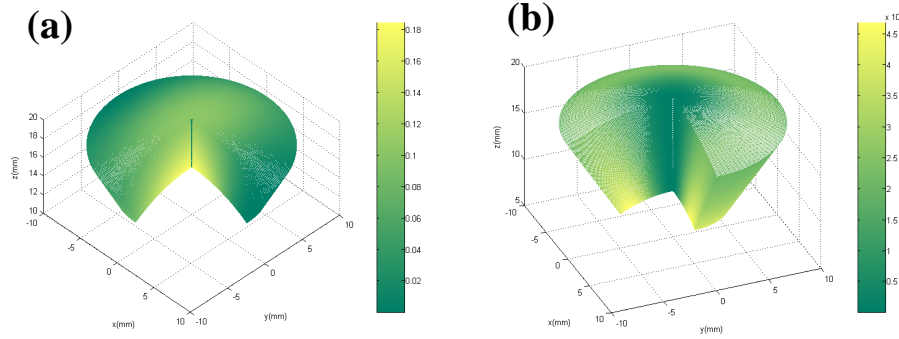
(a)

(b)

Fig. 9. The fields intensities distributions within tapered hollow metal waveguide. The color scheme is such that the engergy density goes from minimum (green) to maximum (yellow). (a) Intensity distributions of TE_{11} mode propagating from $r = 20mm$ to $r = 15mm$ inside tapered hollow metal waveguide with $\theta_0 = \pi/6$. (b) Intensity distributions of TM_{01} mode propagating from $r = 20mm$ to $r = 10mm$ inside tapered hollow metal waveguide with $\theta_0 = \pi/6$.

Figures 9(a) and 9(b) show distinct intensity distributions for TE_{11} and TM_{01} modes inside tapered hollow metal waveguide with $\theta_0 = \pi/6$, respectively. Figure 9(a) reprents the intensity distributions of TE_{11} mode propagating from $r = 20mm$ to $r = 15mm$. Figure 9(b) reprents the intensity distributions of TM_{01} mode propagating from $r = 20mm$ to $r = 10mm$. In order to capture the fields intensities distributions in the hollow core along the propagating direction, we only plot the intensities distributions in the azimuthal angles range from 0 to $3\pi/2$. In the Fig. 9 we observe that all modes appear to be very well confined to the hollow core, i.e., the tapered hollow metallic waveguide can focus a laser beams into a small beam spot . Utilizing the characteristic of the tapered hollow metallic waveguide, some researchs find the waveguide is useful for medial and dental applications [12].

7.   Conclusions

(1) We have developed an exact analytical approach for the description of the electromagnetic fields inside a hollow metallic waveguide with a taper. Analytical expressions for the spatial distributions of electromagnetic field components, attenuation constant, phase constant and wave impedance are derived.

(2) According to our theory the modes configurations inside a tapered hollow metallic waveguide are similar to those in a cylindrical hollow metallic waveguide, but the transmission characteristics and engergy densities distributions along propagating direction have a different behavior. It is shown that all modes run continuously from a propagating through a transition to an evanescent region and the value of the attenuation increases as the distance from the cone vertex and the cone angle desrease. A strict distinction between pure propagating and pure evanescent modes can not be achieved. There is no well-defined cutoff wavelength but rather a cutoff radius. It is interesting to note that the magnitude of the cutoff radius is related to the wavelength and the cone half-angle. The values of attenuation and phase constants for the spherical TE and TM modes inside the tapered hollow metallic waveguide depend on the cone half-angle very seriously. As the cone half-angle decreases, the value of the attenuation increases. The smaller the cone half-angle is, the faster the modes attenuate. This can explain why large taper angle may improve the light throughout in aperture probe which finds an important application in scanning near-field optical microscopy [13].

(3) As follows from our calculations, we find that in the propagating region the attentuation of some modes decays faster than those of others, and one mode after the other reaches cutoff in the tapered hollow metallic waveguide as the distance from the cone vertex decreases.

(4) In the tapered hollow metallic waveguide, light is well confined in the hollow core (air region) because it is reflected back to the core by a metal wall.

Acknowledgments